Nonlinear Dyn
https://doi.org/10.1007/s11071-019-05339-1

ORIGINAL PAPER

Controllable spiking dynamics in cascaded VCSEL-SA photonic neurons

Zhenxue Zhang · Zhengmao Wu · Dan Lu · Guangqiong Xia · Tao Deng

Received: 20 June 2019 / Accepted: 30 October 2019

Abstract We propose a photonic neural system composed of three cascaded vertical-cavity surface-emitting lasers with an embedded saturable absorbers (VCSEL-SAs) and numerically investigate the encoding, propagation and storage characteristics of the spiking patterns in this system. The results show that, with suitable perturbation strength, the first VCSEL-SA (VCSEL-SA1) can convert the stimulus into spike response. Increasing both the perturbation strength and the bias current of active region is beneficial to improve the conversion rate. Moreover, the spiking patterns generated by VCSEL-SA1 can be stably propagated into another two VCSEL-SAs (VCSEL-SA2 and VCSEL-SA3) with a certain delay through adjusting the coupling weight. Additionally, after introducing a feedback into VCSEL-SA1, the fired spiking patterns can be successfully stored in this proposed system. The obtained results can offer great potential for future, brain-inspired ultrafast neuromorphic computing system.

Keywords Vertical-cavity surface-emitting lasers with an embedded saturable absorber (VCSEL-SA) · Controllable spiking dynamics · Conversion rate · Stable propagation · Storage characteristics

Z. Zhang · Z. Wu · G. Xia · T. Deng (✉)
School of Physical Science and Technology, Southwest University, Chongqing 400715, China
e-mail: dengt@swu.edu.cn

D. Lu
Key Laboratory of Semiconductor Materials Science, Institute of Semiconductors, Chinese Academy of Science, Beijing 100083, China

1 Introduction

With the development of artificial intelligence, traditional von Neumann machines have been unable to meet the urgently increasing demands for computing. Compared with traditional digital computing models, neuromorphic systems, which is used to imitate the operation and structure of biological sensing and information processing nervous systems, can solve many more complex computing tasks, such as decision-making, learning and optimization, pattern recognition and sensory information processing [1–6]. As the most basic information processing unit in the biological nervous system, neurons are mainly responsible for the carrying and transmitting signals, sensing changes in the environment, then generating corresponding responses to different stimulus from the outside world [7–10]. Due to the similar responses to external stimulus with biological neurons, different neuronal models including electronic and photonic implementation have been proposed [11–27]. Particularly, neuromorphic photonic models can break through the bandwidth limitation of traditional electronic methods and have become a focus in the neuron-inspired information processing field. In recent years, the excitable lasers, such as conventional vertical-cavity surface-emitting lasers (VCSELs) [13–18], microdisk lasers

Published online: 16 November 2019

[19,20], graphene excitable lasers [21,22], resonant tunneling diode photo-detectors [23], quantum-dot lasers [24,25], and semiconductor lasers with saturable absorber [26,27], have been extensively explored as promising candidates of neuromorphic photonic systems because of the huge application potentials of these devices in optical communication [28], optical interconnection [29] and information processing [30]. Under suitable stimulus, these excitable lasers can all emit the spikes, which are analog in time but digital in amplitude and suitable for resolving complex computing issues. Moreover, they can have a much faster response speed up to 8 orders of magnitude faster than biological neurons. Consequently, this can open a new path to use these excitable lasers in neuro-inspired photonic networks.

Among these excitable lasers, VCSELs have attracted more and more attention in the field of brain-inspired optical information processing since it offers some unique advantages, e.g., low costs, easy integration into three-dimensional arrays and high coupling efficiency to optical fibers [31–34]. Correspondingly, the investigation on VCSEL-based neuromorphic models becomes especially interesting given their special attributes and huge prospects for scaling into network configurations. In recent years, the spiking response characteristics of VCSELs have been experimentally and theoretically investigated, and the spike number and temporal window can be controlled by simply operating the temporal duration and strength of the injected stimulus [16,17]. Furthermore, the spike encoding and storage has been reported numerically in two mutually coupled VCSELs subject to optical pulse injection [35]. Also, the storage of multiple independently addressable phase bits has been realized in an injection-locked semiconductor laser with feedback loop operating in a neuron-like excitable regime [36]. More recently, the propagation of spiking dynamics has been demonstrated between two interlinked VCSELs [13,37]. Above-mentioned results have verified the feasibility of using VCSELs as a neuron model toward neuromorphic photonic networks. Additionally, introducing an extra saturable absorber (SA) into VCSEL can constitute an integrated two-section excitable laser, where the gain medium acts as a temporal integrator and the SA acts as a threshold detector by gating the intensity built up in the cavity by the gain medium [38]. The gain-absorber system based on the vertical cavity design is cascadable [39] and can be employed to constitute a compact platform for studying the excitable spike propagation in semiconductor microphotonic and nanophotonic devices [30]. Moreover, compared with conventional neuron model, VCSEL with saturable absorber (VCSEL-SA), as a simple spike-based leaky integrate-and-fire (LIF) neuron model, is beneficial to generate shorter subnanosecond pulses [30,40–42] and can control the excitability threshold for photonic neuron [43]. Consequently, the photonic neuron configuration based on VCSEL-SA can be used in future brain-inspired neuromorphic computing. However, we have noticed that the investigation on the spiking dynamics in a scalable photonic neuron configuration including three even more VCSEL-SA photonic neurons is relatively scarce.

This work focuses on the spike encoding, propagation and storage characteristics in three cascaded VCSEL-SAs. Firstly, we convert the input stimulus into spike train and discuss the effect of these parameters including the bias current, the input strength and the temporal duration of the input stimulus on the spike encoding characteristics. Secondly, the propagation characteristics of the spiking patterns in three cascaded VCSEL-SAs system are studied numerically. Under suitable optical injection conditions, the spiking responses of first VCSEL-SA (VCSEL-SA1) can be successfully propagated into another two VCSEL-SAs (VCSEL-SA2 and VCSEL-SA3). Finally, the spike storage is demonstrated after adding the feedback loop to VCSEL-SA1 and the influences of the feedback weight and the feedback delay on the storage characteristics of this proposed system have also been numerically analyzed.

2 Theoretical model

Figure 1 shows the schematic diagram of a photonic neural system composed of three cascaded VCSEL-SAs. Besides the VCSEL-SA components, the system includes optical isolator (ISO), fiber coupler (FC), variable attenuator (VA) and delay line (DL), where ISO is used to ensure the unidirectional coupling, VA and DL are, respectively, used to adjust the injection weight and delay. An external perturbation is encoded into continuous light by using an arbitrary waveform generator and a modulator and then is injected into VCSEL-SA1 to emit the spikes. The output of VCSEL-SA1 is divided into two parts by FC2: one is unidirectionally injected

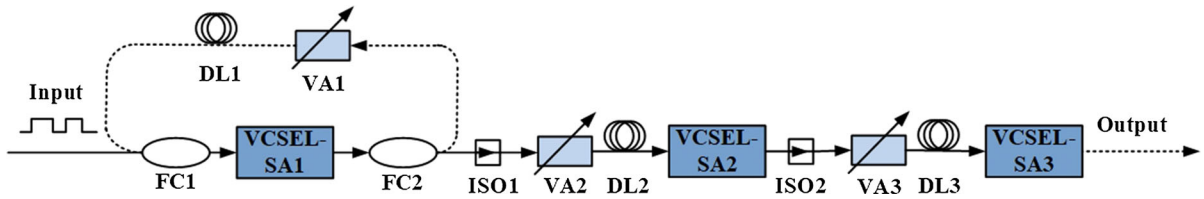

Fig. 1 Schematic illustration of three cascaded VCSEL-SAs. *FC* fiber coupler, *ISO* optical isolator, *VA* variable attenuator, *DL* delay line

into VCSEL-SA2 after passing through ISO1, VA2 and DL2, and the other is used to form a feedback loop via VA1, DL1 and FC1. The output of VCSEL-SA2 is unidirectionally injected into the VCSEL-SA3 via ISO2, VA3 and DL3. Here, the feedback loop is only considered for the storage of spiking patterns.

Based on the coupled rate equations of a two-section excitable laser with gain and SA regions, after taking into account the influence of the external optical pulse injection (stimulus) and optical feedback, the modified rate equations of VCSEL-SA with external perturbation can be described by [40,43]:

$$\begin{aligned}\frac{\mathrm{d}N_{m\mathrm{ph}}}{\mathrm{d}t} &= \Gamma_{ma} g_{ma}(n_{ma} - n_{0ma}) N_{m\mathrm{ph}} \\ &\quad + \Gamma_{ms} g_{ms}(n_{ms} - n_{0ms}) N_{m\mathrm{ph}} \\ &\quad - \frac{N_{m\mathrm{ph}}}{\tau_{m\mathrm{ph}}} + V_{ma}\beta_m B_{mr} n_{ma}^2 \end{aligned} \tag{1}$$

$$\begin{aligned}\frac{\mathrm{d}n_{1a}}{\mathrm{d}t} &= -\Gamma_{1a} g_{1a}(n_{1a} - n_{01a}) \\ &\quad \times \frac{(N_{1\mathrm{ph}} - k\psi(t, \Delta t) - W_f P_1(t - \tau_f))}{V_{1a}} \\ &\quad - \frac{n_{1a}}{\tau_{1a}} + \frac{I_{1a}}{eV_{1a}} \end{aligned} \tag{2}$$

$$\begin{aligned}\frac{\mathrm{d}n_{2a}}{\mathrm{d}t} &= -\Gamma_{2a} g_{2a}(n_{2a} - n_{02a}) \\ &\quad \times \frac{(N_{2\mathrm{ph}} - W_{12} P_1(t - \tau))}{V_{2a}} \\ &\quad - \frac{n_{2a}}{\tau_{2a}} + \frac{I_{2a}}{eV_{2a}} \end{aligned} \tag{3}$$

$$\begin{aligned}\frac{\mathrm{d}n_{3a}}{\mathrm{d}t} &= -\Gamma_{3a} g_{3a}(n_{3a} - n_{03a}) \\ &\quad \times \frac{(N_{3ph} - W_{23} P_2(t - \tau))}{V_{3a}} \\ &\quad - \frac{n_{3a}}{\tau_{3a}} + \frac{I_{3a}}{eV_{3a}} \end{aligned} \tag{4}$$

$$\begin{aligned}\frac{\mathrm{d}n_{ms}}{\mathrm{d}t} &= -\Gamma_{ms} g_{ms}(n_{ms} - n_{0ms}) \frac{N_{m\mathrm{ph}}}{V_{ms}} \\ &\quad - \frac{n_{ms}}{\tau_{ms}} + \frac{I_{ms}}{eV_{ms}} \end{aligned} \tag{5}$$

$$P_m(t) \approx \frac{\eta_{mc}\Gamma_{ma} hc}{\tau_{m\mathrm{ph}}\lambda} N_{m\mathrm{ph}}(t) \tag{6}$$

where the subscripts $m\,(m = 1, 2, 3)$ represent the VCSEL-SA1, VCSEL-SA2 and VCSEL-SA3, respectively, and subscripts a and s represent the active and absorber regions, respectively. $N_{\mathrm{ph}}(t)$ represents the total number of photons in the cavity, $n(t)$ is the number of carriers, and $P(t)$ denotes the output power of the lasers, I is the bias current, which is used to provide the electrical pump. The term $k\psi(t, \Delta t)$ represents the input stimulus coupled into the gain region, where k is the input strength, and Δt is the temporal duration of perturbation. W_f and τ_f is the feedback weight and feedback delay, respectively. W_{12} and W_{23}, respectively, denotes the injection coupling weight from VCSEL-SA1 to VCSEL-SA2 and VCSEL-SA2 to VCSEL-SA3, and τ is the injection coupling delay.

3 Results and discussion

The rate Eqs. (1)–(6) can be numerically solved using the fourth-order Runge–Kutta method. For simplicity, we consider the same parameters for the three VCSEL-SAs. The threshold current is about 2.4 mA for the solitary VCSEL-SA. To operate the two-section laser in the excitable regime, the gain section is biased just below the laser threshold. In this work, we set the bias currents to $I_a = 2.0$ mA and $I_s = 0$ mA for the gain and absorber regions, respectively. The other parameters are summarized in Table 1.

Table 1 Typical VCSEL-SA parameters [43,44]

Parameter	Description	Value
Γ_a	Active region confinement factor	0.06
Γ_s	SA region confinement factor	0.05
τ_a	Active region carrier lifetime (ns)	1
τ_s	SA region carrier lifetime (ps)	100
τ_{ph}	Photon lifetime (ps)	4.8
λ	Lasing wavelength (nm)	850
h	Planck constant	6.634×10^{-34}
V_a	Volume of gain region (m^3)	2.4×10^{-18}
V_s	Volume of SA region (m^3)	2.4×10^{-18}
c	Speed of light ($m\,s^{-1}$)	3×10^8
g_a	Active region differential gain/loss ($m^3.s^{-1}$)	2.9×10^{-12}
g_s	SA region differential gain/loss ($m^3\,s^{-1}$)	14.5×10^{-12}
n_{0a}	Active region transparency carrier density (m^{-3})	1.1×10^{24}
n_{0s}	SA region transparency carrier density (m^{-3})	0.89×10^{24}
B_r	Bimolecular recombination term ($m^3\,s^{-1}$)	1×10^{-15}
β	Spontaneous emission coupling factor	1×10^{-4}
η_c	Output power coupling coefficient	0.4

3.1 Spike encoding

A binary data with the on-off keying (OOK) format is encoded on the continuous light carrier using a Mach–Zehnder (MZ) modulator and an arbitrary waveform generator. The optical signals with added perturbation are injected into the first VCSEL-SA, which can generate the sequence with spike encoding in response to the external stimulus. Figure 2a, b give the spiking response of VCSEL-SA1 to the regular pulse stimulus when the input strength is kept constant of $k = 3 \times 10^3$ and the temporal durations Δt are 10 ns and 15 ns, respectively, where the red dash line denotes the input stimulus and the black solid line denotes the corresponding spiking response. For the case of 0 bit input, the laser outputs are identical to that of laser subject to optical injection without external perturbation. For the case of 1 bit input, the gain carrier concentration is temporally perturbed by the input energy. Once the excitable threshold is exceeded and the SA saturates, the accumulated photon energy can be released in form of a spike and the gain is depleted, which means that a conversion from binary data to spike (BTS) is accomplished. Then VCSEL will experience a refractory period, during which the gain carrier concentration gradually recovers to equilibrium. For different temporal duration Δt and given input strength, the time interval Δt_1 between two consecutive output spikes keeps almost equal even if the number of spikes can increase for large Δt [35], which implies that the temporal duration Δt has no significant impact on the conversion rate once the excitable threshold conditions is achieved [45]. This can be interpreted as that the refractory period, independent of the perturbation's temporal duration, determines the interval Δt_1 (corresponding to the inversion of the BTS conversion rate). Consequently, for a fixed perturbation strength and laser operation parameters, the BTS conversion rate keeps unchanged for different Δt. It should be pointed out that no spikes can be fired during the perturbation time when the temporal duration Δt is shorter than the time interval from the rising edge of bit 1 input to the moment firing the first spike, and then, the BTS conversion will fail. Under above-mentioned condition, the BTS conversion rate of 0.27 Gbps is achieved, as shown in Fig. 2a, b. Figure 2c, d give the spiking response of VCSEL-SA1 to the irregular pulse stimulus, where the stimulus is encoded by a pseudo-random bit sequence. We find that the conversion rate is kept constant for given input strength k and the bias

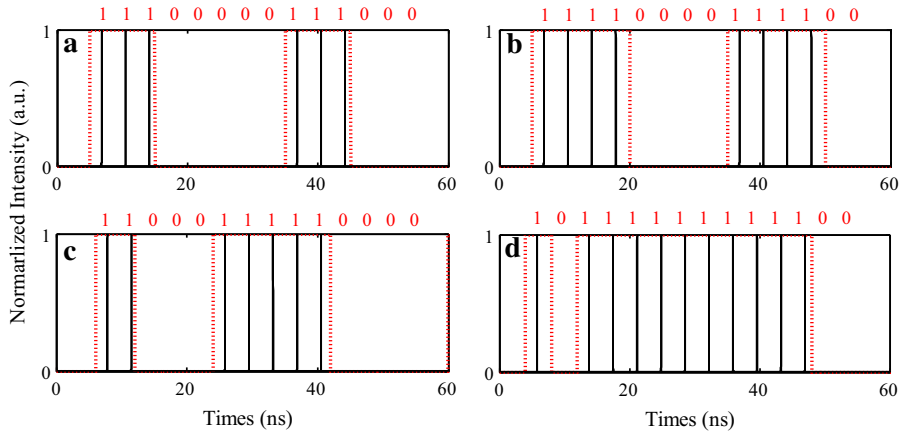

Fig. 2 Time series for the output of VCSEL-SA1 in response to the input stimulus with regular pulses (**a**, **b**) and irregular pulses (**c**, **d**), where red dashed line denotes binary encoded stimulus and black solid line denotes the spiking response trains

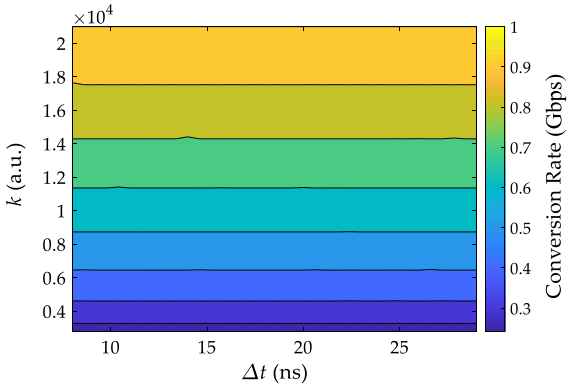

Fig. 3 Two-dimensional map of the conversion rate in the parameters space of k and Δt

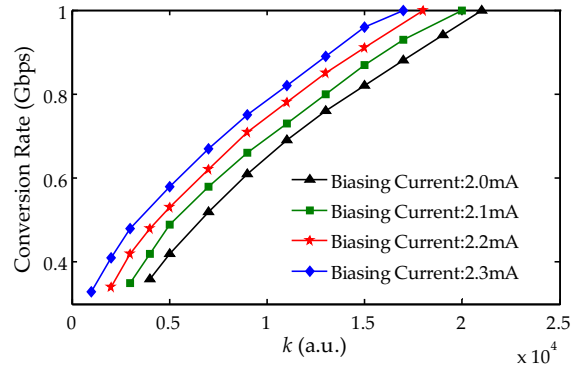

Fig. 4 Conversion rate as a function of input strength k for various biasing currents

current in our simulation, which is consistent of that in Fig. 2a, b.

For further describing the BTS conversion characteristics of this proposed system, Fig. 3 shows the conversion rate of the VCSEL-SA as a function of the input strength k and the temporal duration Δt. From this figure, it can be seen that the conversion rate remains constant for different temporal duration Δt when the input strength is fixed at a certain level, which is consistent of the results in Fig. 2. With the increase of the strength of the input stimulus, the conversion rate can be increased from 0.24 Gbps to 1 Gbps under our simulation conditions, and the higher the stimulus strength is, the higher the conversion rate is. These can be interpreted as the increase of input stimulus decrease the refractory period, which shorten the recovery time of carrier concentration and then is helpful to achieve higher BTS conversion rate. Figure 4 further shows the conversion rate variation as a function of input strength for different bias currents. For a certain conversion rate, a higher input strength is necessary for lower bias current, which may be mainly due to the decrease of refractory period with increasing the bias current. In this work, through controlling the bias current and injection stimulus strength, the BTS conversion rate can be adjusted. Although the maximum conversion rate is limited at 1 Gbps due to the slower of the two carrier lifetimes of the gain and SA [45], the relatively wide variation range of the BTS conversion rate offers the feasibility to future information processing at various operation speeds.

3.2 Propagation of spiking patterns

In the biological neuron networks, the spiking signals excited in neurons are transmitted to neighboring neu-

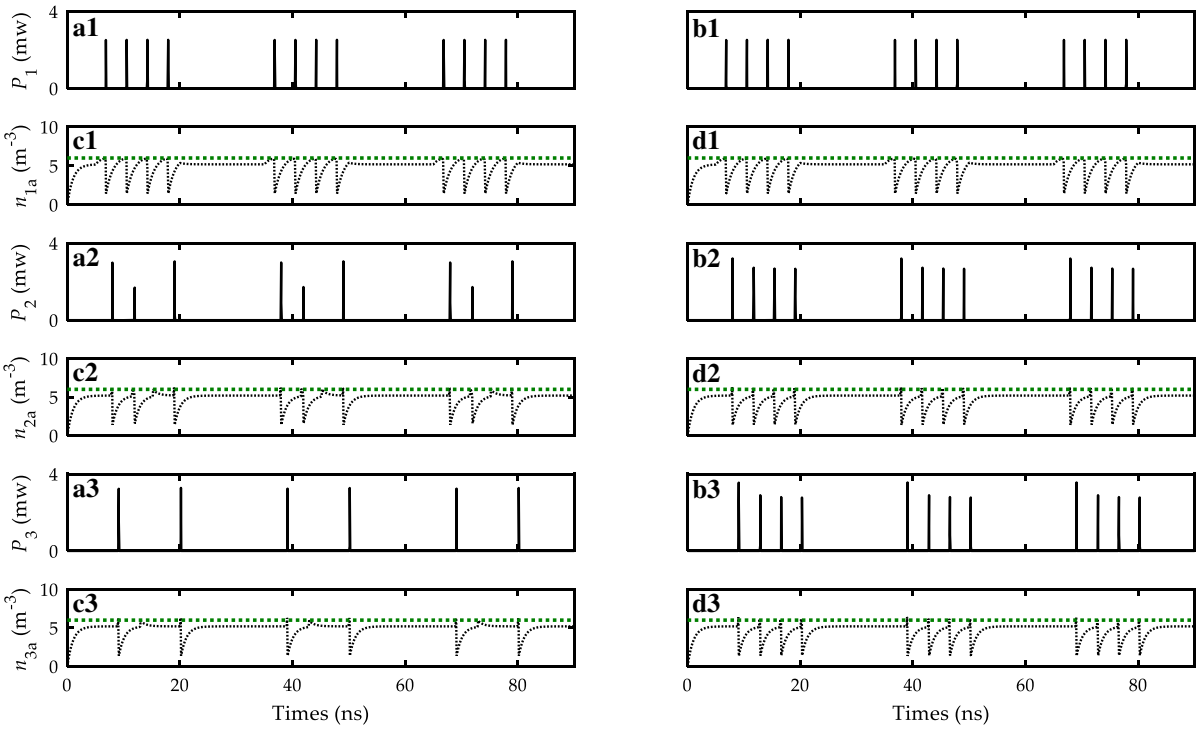

Fig. 5 Spiking outputs (**a**, **b**) and n_a evolution (**c**, **d**) in three cascaded VCSEL-SAs system under different coupling weights of 6.8×10^4 mw^{-1}(**a**, **c**) and 7.4×10^4 mw^{-1}(**b**, **d**), where $\tau = 1$ ns, $k = 3 \times 10^3$

rons through their axons and dendrites, and the communication can be achieved among different neurons. Particularly, the successful communication requires the precise timing of spikes without destroying their temporal structure. For verifying the feasibility of stable propagation of spiking patterns in our proposed cascaded system, Fig. 5 shows the spiking responses and n_a variation under different coupling weights in these three cascaded VCSEL-SAs, where the temporal duration $\Delta t = 15$ ns, $k = 3 \times 10^3$, the feedback weight $W_f = 0$, the coupling delay $\tau = 1$ ns and the coupling weight between lasers is kept equal. For relative low coupling weight of 6.8×10^4 mw^{-1}, the firing spiking pattern in VCSEL-SA1 can be propagated to VCSEL-SA2 and VCSEL-SA3 with missing some spiking information. As shown in Fig. 5a1, VCSEL-SA1 fires four consecutive spike signals in the perturbation time when an external perturbation comes. However, when the spiking events are propagated to VCSEL-SA2 and VCSEL-SA3, only three spikes (Fig. 5a2) and two spikes (Fig. 5a3) can be, respectively, obtained for these two lasers. Obviously, some spiking information has missed during the propagation. When the coupling weight is increased to 7.4×10^4 mw^{-1}, as shown in Fig. 5b1–b3, the spiking events can be propagated to another two VCSEL-SAs and similar responses to the stimulus can be obtained for these three cascaded VCSEL-SAs. These can be explained as follows: The introduction of external perturbation can increase the carrier density n_a in the active region, when n_a accumulates to a certain level exceeding the threshold value approximated by $n_{\text{athresh}} = (\tau_{ph}\Gamma_s g_s n_{0s} + 1)/(\tau_{ph}\Gamma_a g_a) + n_{0a}$ [43], VCSEL-SA can excite spikes. Meanwhile, n_a decreases abruptly and then gradually recovers. The corresponding evolution of n_a has been shown in Fig. 5c, d, where green dashed line denotes the exciting threshold. When the coupling weight is not enough, as shown in Fig. 5c1–c3, the accumulated time of n_a to exceed the exciting threshold, which is corresponding to the refractory period in the VCSEL-SA neuron, will be relatively longer and no spikes can be excited within this time even if new stimulus event comes. With increasing the accumulation time until n_a exceeds the exciting threshold, the new spike will excite. Therefore, some spike information has been missed during the propaga-

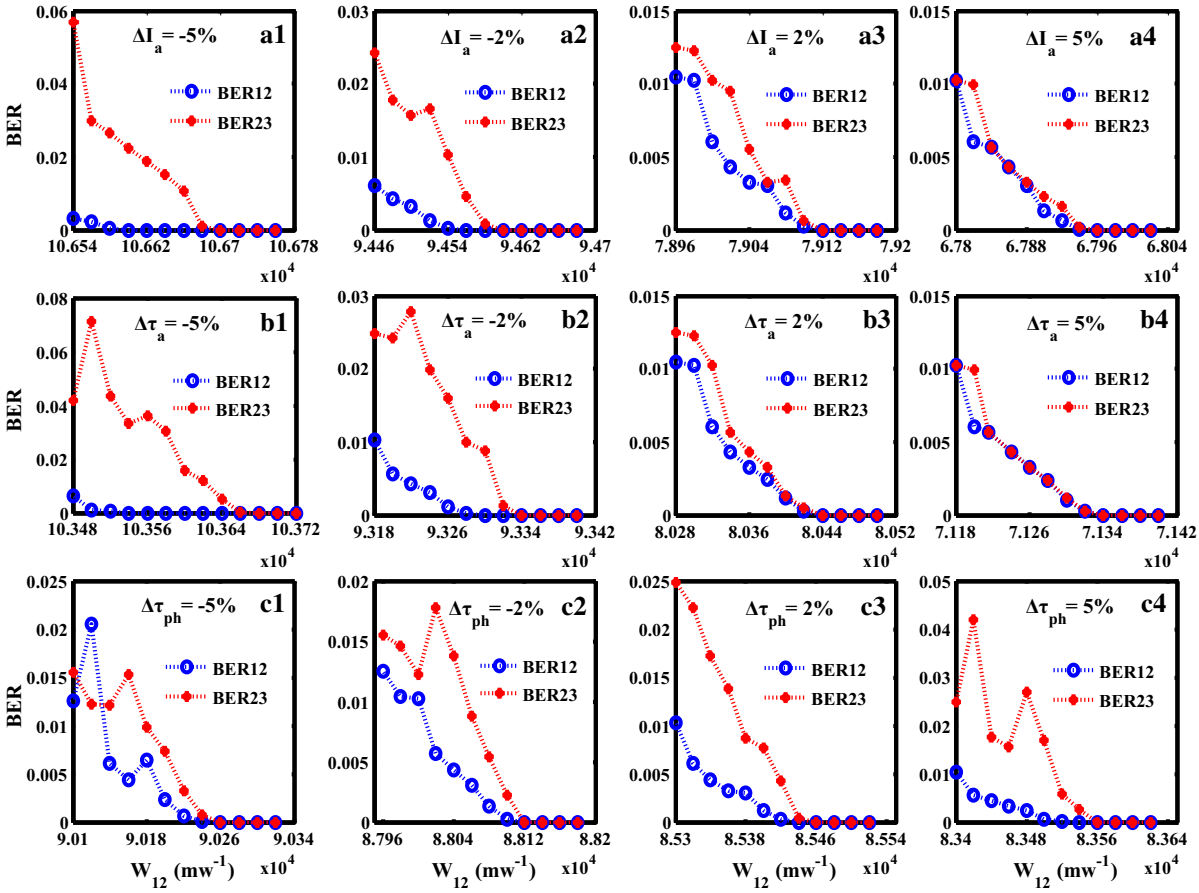

Fig. 6 BERs of spike outputs from three VCSEL-SAs under different parameter mismatches of I_a (**a**), τ_a (**b**) and τ_{ph} (**c**), where the first, second, third and fourth column correspond to -5%, -2%, 2% and 5% parameter mismatches, respectively

tion process. For enough coupling weight, as shown in Fig. 5d1–d3, n_a can rapidly recover to the equilibrium after each spike excites and the spiking patterns can be successfully propagated in three cascaded VCSEL-SAs system. Obviously, the successful propagation of spiking patterns can be guaranteed by adopting suitable coupling weight. It should be noted that the refractory period can be affected by the input power, the coupling weight, the bias current, the detuning frequency between the input light and laser, and so on [46–48]. Particularly, with the increase of the bias current, the accumulation time of the carrier to fire spike will be shortened for a given perturbation above the excitable threshold. Consequently, the refractor period will be shortened with the increase of the bias current [48]. Additionally, from this diagram, it can be observed that, though there exist some differences among the injection signals into three VCSEL-SAs, the laser noise and the injection delay, the three VCSEL-SAs can achieve similar spiking responses with a certain delay and slight different amplitude during the spiking propagation under the case of enough coupling weight.

As well known, it is very difficult to obtain identical lasers in the practical application. For verifying the influences of some parameter mismatches on the spiking dynamics in our proposed system, Fig. 6 shows the variation of the bit error rate (BER) of the spike outputs from three lasers with the coupling weight W_{12} under a fixed coupling weight W_{23} of 9.386×10^4 mw^{-1} and a certain parameter mismatches. Here, a pseudo-random encoded perturbation with $k = 4.6 \times 10^3$ is adopted and some typical parameter mismatches including I_a, τ_a and τ_{ph} are considered. For simplicity, the parameters of VCSEL-SA1 and VCSEL-SA3 are fixed while

some parameters of VCSEL-SA2 are changed, and the relative mismatched parameters are defined as $\Delta I_a = (I_{2a} - I_{1a})/I_{1a} = (I_{2a} - I_{3a})/I_{3a}$, $\Delta\tau_a = (\tau_{2a} - \tau_{1a})/\tau_{1a} = (\tau_{2a} - \tau_{3a})/\tau_{3a}$, and $\Delta\tau_{ph} = (\tau_{2\mathrm{ph}} - \tau_{1\mathrm{ph}})/\tau_{1\mathrm{ph}} = (\tau_{2\mathrm{ph}} - \tau_{3ph})/\tau_{3ph}$. BER12 is the BER between VCSEL-SA1 and VCSEL-SA2, and BER23 is the BER between VCSEL-SA2 and VCSEL-SA3. From this diagram, one can see that, under a certain parameter mismatches from -5% to 5%, BER23 are almost higher than BER12 for relatively small coupling weight W_{12}, and both BER12 and BER23 will tend to a low level for enough large W_{12}. Obviously, the parameter mismatches have some influence on the spiking propagation performance in this proposed system. Moreover, increasing the coupling weight can enhance the spiking propagation robustness to the parameter mismatches [49,50].

3.3 Storage of spiking patterns

Finally, we discuss the storage properties of spiking patterns by adding the feedback loop to the first laser. Figure 7 plots the input stimulus (red dashed line) and the output responses of three VCSEL-SAs, where the feedback parameters are fixed at $W_f = 7.5\times10^4$ mw^{-1} and $\tau_f = 14$ ns, the injection coupling strength is set as 7.5×10^4 mw^{-1} and the injection perturbation is encoded with a rectangular pulse with $k = 3 \times 10^3$ and $\Delta t = 10$ ns. When an external perturbation arrives, VCSEL-SA1 repetitively fires three-spike bursts with a fixed time interval, which is corresponding to the feedback delay, as shown in Fig. 7b. This can be interpreted as that, upon the external perturbation, VCSEL-SA1 firstly fired three spikes, which will repetitively stimulate the VCSEL-SA1 due to the added feedback loop. Under suitable injection coupling weight as discussed in the previous section, the consecutive spiking responses will be successfully propagated to another two VCSEL-SAs except extra injection delay, as shown in Fig. 7c, d. Under this condition, the spike information can be successfully stored in the cascaded system, which can be used to regenerate the complex spiking patterns.

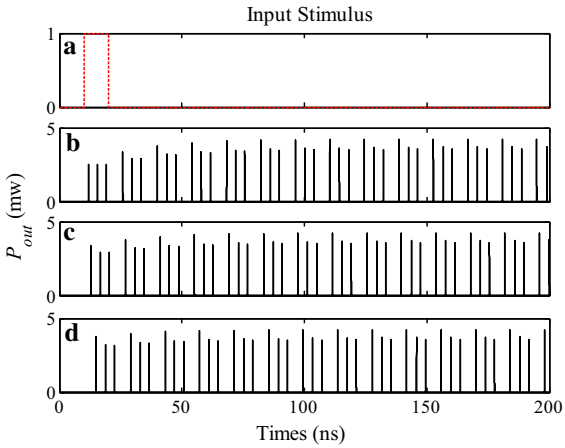

Fig. 7 Storage of spiking patterns in three cascaded VCSEL-SAs with optical feedback for the coupling delay $\tau = 1$ ns

For realizing the storage of spiking patterns in our proposed cascaded system, two important parameters need to be controlled, namely the feedback weight W_f and the feedback delay τ_f. Therefore, it is necessary to investigate the effects of the W_f and τ_f on the storage characteristics. Figure 8a1–d1 shows the time series at the output of VCSEL-SA1 for different values of W_f and a fixed τ_f, where $k = 3\times10^3$, $\Delta t = 3$ ns. It should be pointed out that only the output of VCSEL-SA1 is presented for simplicity after considering similar responses of three lasers to external perturbation under suitable optical injection conditions. From these diagrams, it can be seen that, for relative low the feedback weight of $W_f = 6.2\times10^4$ mw^{-1}, VCSEL-SA1 generates only two spikes over long timescales, as shown in Fig. 8a1, which indicates that the spike codes cannot be stored in the system. With increasing W_f, the spiking pattern can be stored perfectly over long timescales and the consecutive spiking sequence can be obtained (see in Fig. 8b1–d1). These can be interpreted as that, the firstly excited spike from VCSEL-SA1 is fed back the laser as a new stimulus after a feedback delay, which can fire new spike once the spiking excitation condition is achieved. Under the weak feedback, the accumulated carrier density can exceed the exciting threshold after the first feedback delay and VCSEL-SA1 excites a new spike. However, after second or more feedback delays, the accumulated carrier density is almost lower than the exciting threshold, so the excited spike is only stored within two delay period and then disappears. With the increase of W_f, the refractory period of laser will be decreased and the recovery rate of carrier will be improved. Once W_f exceeds a certain threshold level, new spike will be consecutively fired after each feedback delay. Under our simulation conditions, a threshold value of $W_f = 6.42\times10^4$mw^{-1} is obtained for the

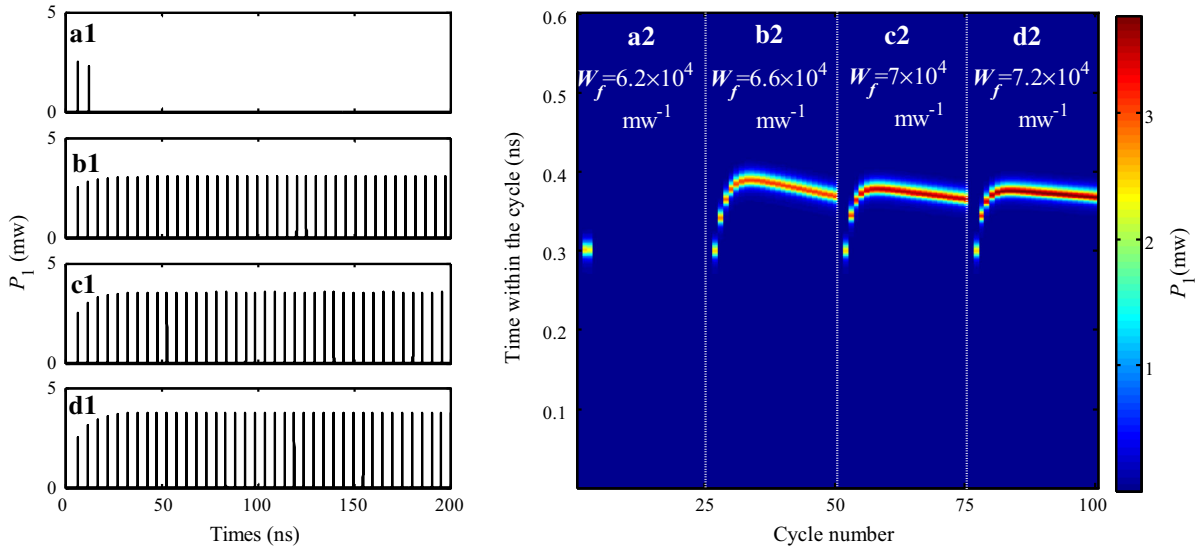

Fig. 8 Numerically calculated time series of the VCSEL-SA1 and corresponding temporal maps for different values of W_f : **a1** 6.2×10^4 mw^{-1}, **b1** 6.6×10^4 mw^{-1}, **c1** 7×10^4 mw^{-1}, **d1** 7.2×10^4 mw^{-1}. The other parameters are $k = 3 \times 10^3$, $\Delta t = 3$ ns and $\tau_f = 5$ ns

stable storage of spiking patterns. To further verify the feasibility of the storage of spiking patterns, the calculated (color-coded) temporal maps corresponding to the time series in Fig. 8a1–d1 are displayed in Fig. 8a2–d2 after referring to the same form as Fig. 5 in Ref. [13], where each one describes 25 superimposed time traces. In these maps, the color code indicates the increasing strength (corresponding to the height of the spike) from blue to red, where the red color denotes high-intensity spikes and the blue corresponds to the steady state. Under our external perturbation condition, only one spike is fired when the perturbation arrives and the fired spike will be used as a new stimulus signal for the VCSEL-SA1 with feedback. The time interval between consecutive two spikes can change for different W_f. In our simulation, the mean time interval between two consecutive spikes in a time window consisted of 25 consecutive perturbation events is taken as a folding parameter (the time window of each superimposed time trace) for these maps, and the folding parameter for different values of W_f is 5.29 ns, 5.15 ns, 5.11 ns, 5.09 ns, respectively. Figure 8a2–d2 clearly shows that the spiking pattern generated by VCSEL-SA1 can be repeatedly stored with a period corresponding to the feedback delay under relatively large feedback weight.

Figure 9 plots the time series of VCSEL-SA1 with a fixed W_f and varied feedback delay from 3.5 ns to 4.2 ns. When an external optical signal with encoded perturbation with $k = 3 \times 10^3$ and $\Delta t = 3$ns is injected into the VCSEL-SA1, the laser excites a spike in response to the stimulus. For the case of $\tau_f = 3.5$ ns (Fig. 9a1), the accumulated carrier density within each feedback delay will gradually decrease after each releasing of spike, then the excited spike is only stored within several feedback delays. With increasing feedback delay to 3.8 ns (Fig. 9b1), 4 ns (Fig. 9c1) and 4.2 ns (Fig. 9d1), the stable storage of spiking patterns can be achieved. These phenomena are mainly because increasing the feedback delay is beneficial to accumulate the carrier after each spike exciting for laser and the exciting threshold is easier to be exceeded. Moreover, a threshold value of $\tau_f = 3.59$ ns can be obtained for the stable storage of spiking pattern in this simulation. Similar to Figs. 8a2–d2, 9a2–d2 illustrate the temporal maps corresponding to the time series in Fig. 9a1–d1. Due to the influence of feedback delay on the response time of the laser to external perturbation, the folding parameters are respectively set as 3.73 ns, 3.95 ns, 4.13 ns, 4.32 ns for Fig. 9a1–d1. Obviously, in our simulation conditions, the successful storage of spiking patterns can be achieved once the feedback delay exceeds

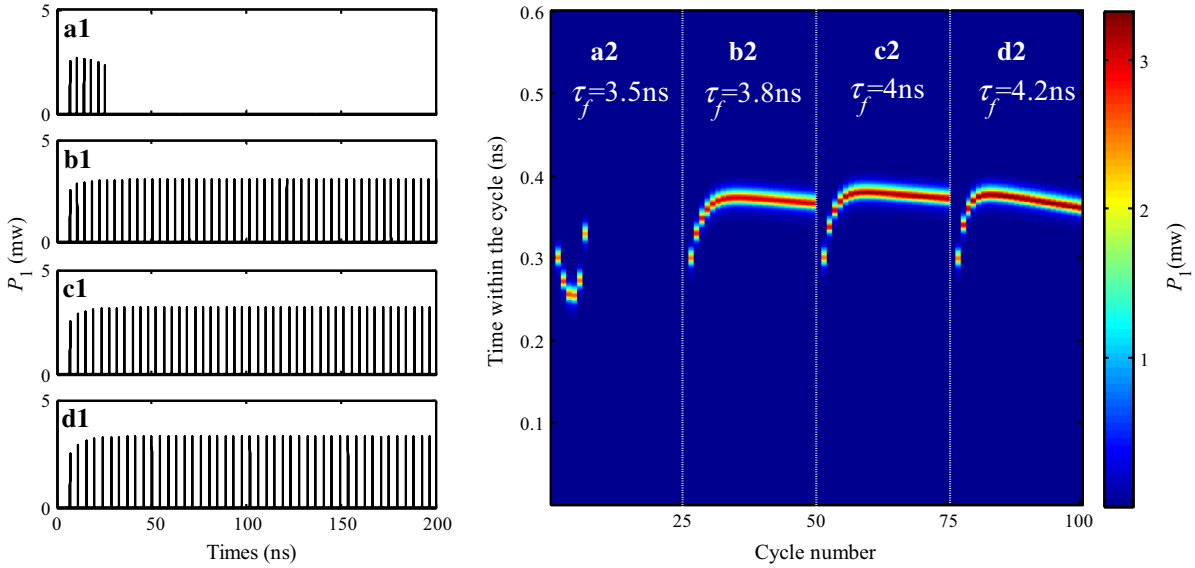

Fig. 9 Numerically calculated time series of VCSEL-SA1 and corresponding temporal maps for different values of τ_f: **a1** 3.5 ns, **b1** 3.8 ns, **c1** 4 ns, **d1** 4.2 ns. The other parameters are $k = 3 \times 10^3$, $\Delta t = 3$ ns, $W_f = 7 \times 10^4 \text{mw}^{-1}$

a certain threshold. Combined Fig. 8 with Fig. 9, it is clear that the feedback weight and the feedback delay have significant impact on the storage characteristics in our cascaded system and larger values of τ_f and W_f are beneficial for spike storage in the system. These can offer an effective controlling path to the storage of spiking patterns.

4 Conclusions

In summary, we propose the three-cascaded VCSEL-SAs system and investigates its spiking dynamic characteristics. Firstly, we demonstrate the spike encoding of VCSEL-SA under regular and irregular perturbations, respectively, and the conversation from binary code to spike (BTS) has been achieved. With increasing the perturbation strength, the conversion rate can be improved in our simulation. For a fixed conversion rate, a relative high perturbation strength is required for the lower bias current. Next, the spiking patterns excited by VCESL-SA1 can be stably propagated into another two VCSEL-SAs for enough coupling weight in our system and similar spiking response to external perturbation can be obtained for each VCSEL-SA. Finally, we discuss the storage characteristics of this system after introducing added feedback loop. The feedback weight and the feedback delay have significant impact on the storage characteristics. The relatively larger feedback weight and feedback delay are helpful to store the spiking patterns. These findings open a window to control the spike encoding, spike propagation and spike storage in the VCSEL-SA photonic neural system, which can offer exciting prospects for the prompting the application of VCSEL-SA in the ultrafast photonic neuromorphic system and brain-inspired photonic information processing.

Acknowledgements This work was supported by National Natural Science Foundation of China (NSFC) (61775184, 61875167); Natural Science Foundation of Chongqing City (CSTC 2019jcyj-msxm X0136).

Compliance with ethical standards

Conflict of interest The authors declare that they have no conflict of interest.

References

1. Nahmias, M.A., Shastri, B.J., Tait, A.N., Lima, T.F.D., Prucnal, P.R.: Neuromorphic photonics. Opt. Photon. News **29**, 34–41 (2018)
2. Feldmann, J., Youngblood, N., Wright, C.D., Bhaskaran, H., Pernice, W.H.P.: All-optical spiking neurosynaptic networks with self-learning capabilities. Nature **569**, 208–214 (2019)

3. Lima, T.F.D., Shastri, B.J., Tait, A.N., Nahmias, M.A., Prucnal, P.R.: Progress in neuromorphic photonics. Nanophoton. **6**, 577–599 (2017)
4. Arena, P., Calí, M., Patané, L., Portera, A., Spinosa, A.G.: A CNN-based neuromorphic model for classification and decision control. Nonlinear Dyn. **95**, 1999–2017 (2019)
5. Shen, Y., Harris, N.C., Skirlo, S., Prabhu, M., Baehr-Jones, T., Hochberg, M., Sun, X., Zhao, S.J., Larochelle, H., Englund, D., Soljačić, M.: Deep learning with coherent nanophotonic circuits. Nat. Photon. **11**, 441–446 (2017)
6. Lin, X., Rivenson, Y., Yardimci, N.T., Veli, M., Luo, Y., Jarrahi, M., Ozcan, A.: All-optical machine learning using diffractive deep neural networks. Science **361**, 1004–1008 (2018)
7. Jia, B., Wu, Y.C., He, D., Guo, B.H.: Dynamics of transitions from anti-phase to multiple in-phase synchronizations in inhibitory coupled bursting neurons. Nonlinear Dyn. **93**, 1599–1618 (2018)
8. Betley, N.J., Xu, S.J., Cao, Z.F.H., Gong, R., Magnus, C.J., Yu, Y., Sternson, S.M.: Neurons for hunger and thirst transmit a negative-valence teaching signal. Nature **521**, 180–185 (2015)
9. Guo, F., Yu, W., Jung, H.J., Abruzzi, K.C., Luo, W.F., Griffith, L.C., Rosbash, M.: Circadian neuron feedback controls the Drosophila sleep-activity profile. Nature **536**, 292–297 (2016)
10. Kuhara, A., Okumura, M., Kimata, T., Tanizawa, Y., Takano, R., Kimura, K.D., Inada, H., Matsumoto, K., Mori, I.: Temperature sensing by an olfactory neuron in a circuit controlling behavior of C. elegans. Science **320**, 803-807 (2008)
11. Hsu, J.: IBM's new brain. IEEE Spectr. **51**, 17–19 (2014)
12. Lim, H., Ahn, H.W., Kornijcuk, V., Kim, G., Seok, J.Y., Kim, I., Hwang, C.S., Jeong, D.S.: Relaxation oscillator-realized artificial electronic neurons, their responses, and noise. Nanoscale **8**, 9629–9640 (2016)
13. Deng, T., Robertson, J., Wu, Z.M., Xia, G.Q., Lin, X.D., Tang, X., Wang, Z.J., Hurtado, A.: Stable propagation of inhibited spiking dynamics in vertical-cavity surface-emitting lasers for neuromorphic photonic networks. IEEE Access **6**, 67951–67958 (2018)
14. Xiang, S.Y., Wen, A.J., Pan, W.: Emulation of spiking response and spiking frequency property in VCSEL-based photonic neuron. IEEE Photon. J. **8**, 1504109 (2016)
15. Xiang, S.Y., Zhang, H., Guo, X.X., Hao, Y.: Cascadable neuron-like spiking dynamics in coupled VCSELs subject to orthogonally polarized optical pulse injection. IEEE J. Sel. Top. Quantum Electron. **23**, 1700207 (2017)
16. Hurtado, A., Javaloyes, J.: Controllable spiking patterns in long-wavelength vertical cavity surface emitting lasers for neuromorphic photonics systems. Appl. Phys. Lett. **107**, 241103 (2015)
17. Robertson, J., Deng, T., Javaloyes, J., Hurtado, A.: Controlled inhibition of spiking dynamics in VCSELs for neuromorphic photonics: theory and experiments. Opt. Lett. **42**, 1560–1563 (2017)
18. Li, Q., Wang, Z., Cui, C., Li, R.Q., Li, Y., Liu, B., Wu, C.Q.: Simulation the spiking response of VCSEL-based optical spiking neuron. Opt. Commun. **18**, 327–332 (2018)
19. Van Vaerenbergh, T., Alexander, K., Dambre, J., Bienstman, P.: Excitation transfer between optically injected microdisk lasers. Opt. Express **21**, 28922–28932 (2013)
20. Alexander, K., Van Vaerenbergh, T., Fiers, M., Mechet, P., Dambre, J., Bienstman, P.: Excitability in optically injected microdisk lasers with phase controlled excitatory and inhibitory response. Opt. Express **21**, 26182–26191 (2013)
21. Shastri, B.J., Nahmias, M.A., Tait, A.N., Rodriguez, A.W., Wu, B., Prucnal, P.R.: Spike processing with a graphene excitable laser. Sci. Rep. **6**, 19126 (2016)
22. Shastri, B.J., Nahmias, M.A., Tait, A.N., Prucnal, P.R.: Simulations of a graphene excitable laser for spike processing. Opt. Quantum Electron. **46**, 1353–1358 (2014)
23. Romeira, B., Javaloyes, J., Ironside, C.N., Figueiredo, J.M.L., Balle, S., Piro, O.: Excitability and optical pulse generation in semiconductor lasers driven by resonant tunneling diode photo-detectors. Opt. Express **21**, 20931–20940 (2013)
24. Kelleher, B., Goulding, D., Hegarty, S.P., Huyet, G., Cong, D.Y., Martinez, A., Lemaître, A., Ramdane, A., Fischer, M., Gerschütz, F., Koeth, J.: Excitable phase slips in an injection-locked single-mode quantum-dot laser. Opt. Lett. **34**, 440–442 (2009)
25. Olejniczak, L., Panajotov, K., Thienpont, H., Sciamanna, M.: Self-pulsations and excitability in optically injected quantum-dot lasers: impact of the excited states and spontaneous emission noise. Phys. Rev. A **82**, 023807 (2010)
26. Perego, A.M., Lamberti, M.: Collective excitability, synchronization, and array-enhanced coherence resonance in a population of lasers with a saturable absorber. Phys. Rev. A **94**, 033839 (2016)
27. Zhang, Y.H., Xiang, S.Y., Guo, X.X., Wen, A.J., Hao, Y.: Polarization-resolved and polarization-multiplexed spike encoding properties in photonic neuron based on VCSEL-SA. Sci. Rep. **8**, 1–9 (2018)
28. Mesaritakis, C., Kapsalis, A., Bogris, A., Syvridis, D.: Artificial neuron based on integrated semiconductor quantum dot mode-locked lasers. Sci. Rep. **6**, 39317 (2016)
29. Tait, A.N., Nahmias, M.A., Shastri, B.J., Prucnal, P.R.: Broadcast and weight: An integrated network for scalable photonic spike processing. IEEE J. Lightw. Technol. **32**, 4029–4041 (2014)
30. Barbay, S., Kuszelewicz, R., Yacomotti, A.: Excitability in a semiconductor laser with saturable absorber. Opt. Lett. **36**, 4476–4478 (2011)
31. Koyama, F.: Recent advances of VCSEL photonics. IEEE J. Lightwave Technol. **24**, 4502–4513 (2006)
32. Zhong, D.Z., Ji, Y.Q., Luo, W.: Controllable optoelectric composite logic gates based on the polarization switching in an optically injected VCSEL. Opt. Express **23**, 29823–29833 (2015)
33. Jayaprasath, E., Wu, Z.M., Sivaprakasam, S., Xia, G.Q.: Observation of additional delayed-time in chaos synchronization of uni-directionally coupled VCSELs. Chaos **28**, 123103 (2018)
34. Deng, T., Xia, G.Q., Wu, Z.M.: Broadband chaos synchronization and communication based on mutually coupled VCSELs subject to a bandwidth-enhanced chaotic signal injection. Nonlinear Dyn. **76**, 399–407 (2014)
35. Zhang, Y.H., Xiang, S.Y., Gong, J.K., Guo, X.X., Wen, A.J., Hao, Y.: Spike encoding and storage properties in mutually coupled vertical-cavity surface-emitting lasers subject to optical pulse injection. Appl. Opt. **57**, 1731–1737 (2018)

36. Bruno, G., Julien, J., Giovanna, T., Stéphane, B.: Topological solitons as addressable phase bits in a driven laser. Nat. Commun. **6**, 5915 (2015)
37. Deng, T., Robertson, J., Hurtado, A.: Controlled propagation of spiking dynamics in vertical-cavity surface-emitting lasers: towards neuromorphic photonic network. IEEE J. Sel. Top. Quantum Electron. **23**, 1800408 (2017)
38. Prucnal, P.R., Shastri, B.J., Lima, T.F., Nahmias, M.A., Tait, A.N.: Recent progress in semiconductor excitable lasers for photonic spike processing. Adv. Opt. Photon. **8**, 228–299 (2016)
39. Nahmias, M.A., Tait, A.N., Shastri, B.J., Lima, T.F., Prucnal, P.R.: Excitable laser processing network node in hybrid silicon: analysis and simulation. Opt. Express **23**, 26800–26813 (2015)
40. Nugent, D.G.H., Plumb, R.G.S., Fisher, M.A., Davies, D.A.O.: Self-pulsation in vertical-cavity surface-emitting lasers. Electron. Lett. **31**, 43–44 (1995)
41. Shchukin, V.A., Ledentsov, N.N., Qureshi, Z., Ingham, J.D., Penty, R.V., White, I.H., Nadtochy, A.M., Maximov, M.V., Blokhin, S.A., Karachinsky, L.Ya., Novikov, I.I.: Digital data transmission using electro-optically modulated vertical-cavity surface-emitting laser with saturable absorber. Appl. Phys. Lett. **104**, 051125 (2014)
42. Hoogland, S., Dhanjal, S., Tropper, A.C., Roberts, J.S., Haring, R., Paschotta, R., Morier-Genoud, F., Keller, U.: Passively mode-locked diode-pumped surface-emitting semiconductor laser. IEEE Photon. Technol. Lett. **12**, 1135–1137 (2000)
43. Nahmias, M.A., Shastri, B.J., Tait, A.N., Prucnal, P.R.: A leaky integrate-and-fire laser neuron for ultrafast cognitive computing. IEEE J. Sel. Top. Quantum Electron. **19**, 1800212 (2013)
44. Shastri, B.J., Nahmias, M.A., Tait, A.N., Wu, B., Prucnal, P.R.: SIMPEL: Circuit model for photonic spike processing laser neurons. Opt. Express **23**, 8029–8044 (2015)
45. Ma, P.Y., Shastri, B.J., Lima, F.T.D., Tait, A.N., Nahmias, M.A., Prucnal, P.R.: All-optical digital-to-spike conversion using a graphene excitable laser. Opt. Express **25**, 33504–33513 (2017)
46. Selmi, F., Braive, R., Beaudoin, G., Sagnes, I., Kuszelesicz, R., Barbay, S.: Relative refractory period in an excitable semiconductor laser. Phys. Rev. Lett. **112**, 183902 (2014)
47. Garbin, B., Dolcemascolo, A., Prati, F., Javaloyes, J., Tissoni, G., Barland, S.: Refractory period of an excitable semiconductor laser with optical injection. Phys. Rev. E **95**, 012214 (2017)
48. Selmi, F., Braive, R., Beaudoin, G., Sagnes, I., Kuszelewicz, R., Barbay, S.: Neuromimetic dynamics in a micropillar laser with saturable absorber. 2015 European Conference on Lasers and Electro-Optics-European Quantum Electronics Conference. Paper EF_8_1 (2015)
49. Kistler, W.M.: Stable propagation of activity pulses in populations of spiking neurons. Neural Comput. **14**, 987–997 (2002)
50. Prucnal, P.R., Shastri, B.J.: Neuromorphic Photonics. CRC Press, Boca Raton (2017)